The SCEC Community Geodetic Model V1: Horizontal Velocity Grid

David T. Sandwell

Yuehua Zeng

Zheng-Kang Shen

Brendan Crowell

Jessica Murray

Rob McCaffrey

Xiaohua Xu

Draft V2: October 17, 2016

Abstract

The SCEC community is constructing and updating a suite of models for the Southern California region to facilitate cross-disciplinary research (CFM, CVM, CGM, CSM, and CRM). Here we are concerned with the development of the Community Geodetic Model (CGM). Eventually the CGM will consist of vector deformation time series at ~1 km resolution, and better than seasonal sampling. As a first step we are constructing a 0.01˚ resolution grid of horizontal vector velocities and 2-D tensor strain rate covering the areas of interest to SCEC scientists. Our approach is to first assemble 15 available velocity and strain rate models for the SCEC region. There were 4 main approaches to model construction: isotropic interpolation, interpolation guided by known faults, interpolation of a rheologically-layered lithosphere, and model fitting using deep dislocations in an elastic layer or a half space. We then evaluate the 15 strain rate models in terms of roughness, cross correlation, seismicity rate, and SHmax to select a subset of 9 usable models. Since all the models are based on slightly different geodetic data and use a variety of reference frames, we re-gridded velocities from the 9 models at a 0.01˚ grid spacing. This is accomplished by forcing each velocity model to match the best available GPS velocity data for the region. The 9 velocity models were averaged and their standard deviation was also computed. Standard deviations are generally small (< 0.5 mm/yr) in areas of good GPS coverage; areas of large standard deviation illustrate where InSAR velocities will contribute most. This uniform velocity is a first step in the development of the full 3-D time dependent CGM. This result is important for seismic hazard evaluation as well as InSAR time series analysis. As new GPS and InSAR data become available this SCEC community model will continue to evolve. The full compilation of the GPS velocity data, the contributed models, and the consensus products will be available on the SCEC web site.

Introduction

SCEC is constructing and updating a suite of community models for the Southern California Region to facilitate cross-disciplinary research. Currently they include: the Community Fault Model (CFM), the Community Velocity Model (CVM), the Community Geodetic Model (CGM), the Community Stress Model and eventually the Community Rheology Model (CRM) [Jordan et al., 2016]. Here we are concerned with the development of the CGM. Eventually the CGM will consist of vector deformation time series at ~1 km resolution and better than seasonal sampling. The CGM draws upon expanded Global Positioning System (GPS) coverage, new SAR missions, and maturing data analysis techniques that leverage the complimentary features of both data types. By adopting a community-driven approach, we bring together the broad expertise and diverse perspectives needed to explore the effect of modeling choices and provide a window into the scope of epistemic uncertainty.

Previously SCEC has developed the Southern California Crustal Motion Map [e.g., V4.0 Shen et al., 2011], which consists of the motion of a large number of geodetic monuments in Southern California. These motions were estimated from a combination of EDM, GPS, and VLBI data. The science and hazard communities also require a dense grid of vector surface velocities to compute, for example seismic moment accumulation rate as well as crustal strain rate, for hazard analysis [e.g., UCERF3; Field et al., 2014]. Strain rate along faults, which can have large amplitude (100 - 3000 nanostrain per year), is concentrated within 10-50 km of the fault trace depending on the locking depth of the fault (Appendix A). The second process producing strain rate is widespread deformation of the crustal blocks. This strain rate generally has much lower amplitude (10 – 100 nanostrain per year) and can be masked by the larger near-fault component. Both of these components of strain rate may help in forecasting earthquakes. The near-fault strain rate is proportional to the long-term slip rate across the fault divided by the thickness of the locked zone. Mapping this near-field strain rate

may help to refine our physical understanding of the recurrence interval of major earthquakes. The widespread strain internal to the crustal blocks may be an indicator of stress rate, which can produce intermediate (magnitude 5-6) and sometimes large earthquakes (e.g., the 1992 Landers M7.2 rupture).

Geodetic measurements can be used to estimate both the moment and strain accumulation rate although the spacing of the measurements must be less than the locking depth (~8 km) to achieve accurate estimates. When the measurements are spatially dense, the strain rate can be measured quite accurately. However the typical spacing of GPS data in California is about 10 km [Wei et al., 2010] so in most cases the GPS data cannot adequately resolve the strain rate unless other information such as the location of the major faults is also available. Because of this inadequate sampling, published strain rate maps sometimes differ by an order of magnitude. A previous analysis of strain-rate maps produced by 16 different research groups using primarily the same GPS velocity measurements, reveals that modeled strain rate can differ by factors of 5 to 8 times, with the largest differences occurring along the most active faults [Hearn et al., 2010].

This report is a continuation of the effort to arrive at a consensus CGM gridded horizontal velocity model, which also provides a tensor strain rate model. Our approach is to: (1) assemble all available velocity and strain rate models for the SCEC region; (2) evaluate the strain rate models in terms of roughness, cross correlations, seismicity rate, and SHmax [Yang and Haukkson, 2013]; (3) select a subset of “best” models; (4) use a remove/restore analysis to force all the models to match the best available GPS velocity data; and (5) average the velocity grids and strain tensor grids to arrive at a consensus CGM including model uncertainties.

The final model consists of 1-km resolution grid of north and east velocities and velocity uncertainties as well as a horizontal strain rate tensor and strain rate uncertainty. This uniform velocity is just a first step in the development of the full 3-D time dependent CGM. Nevertheless this compilation is important for hazard analysis as well as more practical uses such as isolating the vertical deformation

in InSAR time series. As new GPS and InSAR data become available the SCEC community will update this models.

Assembly

The models considered for this initial release are velocity and strain rate models of a large region of California contributed by 15 groups [Figure 1 and Table 1]. Most of the models have matching publication although some of the publications are very old (e.g., 16 yr) and were based on poorer quality data than is available today. Therefore we asked each group to provide an updated model based on the latest geodetic data. There were 4 main approaches to model construction: isotropic interpolation, interpolation guided by known faults, interpolation of a rheologically-layered lithosphere, and model fitting using deep dislocations in an elastic layer or a half space. The details of the construction of each model are provided in the publications listed in Table 1. Since the models are all based on slightly different geodetic data and use a variety of reference frames (e.g. ITRF2005, SNARF, SAF-zeroed), it is difficult to compare the velocity grids directly. Therefore initially we compute strain rates (or use supplied strain rates) for model evaluation. All models were re-gridded at a 0.01˚ (~1 km) grid spacing and tensor strain rate was computed as described in Appendix B. From these we computed various products of second invariant, azimuth of maximum compression, and dilatation (Appendix B).

After the evaluation of the 15 strain rate contributions, we need to construct matching velocity grids. As described in greater detail below, this is accomplished by forcing each velocity model to match the best available GPS velocity data for the region. The core of the horizontal GPS velocities were compiled by Zeng and Shen [2016b] and McCaffrey et al., [2013]. These were augmented by regional compilations from Crowell et al., [2013] and Murray et al. [20XX]. Of course each of the three main data sets have many contributions from throughout the geodetic community including long time series from the Plate Boundary observatory. There are 1339 unique horizontal vector velocities and

uncertainties as plotted in Figure 1. Again these data will provide the overall framework for the gridded CGM products.

Table 1. Velocity and strain rate models contributed to the CGM

NAME	MODEL VEL	MODEL STRAIN_RATE	STRAIN RATE EVAL.			PUBLICATION
			rms	SHmax	corr	
becker	O	X	81	14.5	.76	Platt and Becker, 2010
bird	X	X	183	19.2	.58	Petersen et al., 2014; Field et al., 2014
bormann_hammond	X	X	99	19.2	.64	Johnson et al., 2013
gpsgridder	X	X	109	17.1	.77	Sandwell and Wessel, 2016
hackl	X	X	134	26.1	.70	Hackl, 2009
holt	X	X	124	18.3	.73	Flesch et al., 2000
kreemer	X	X	152	20.4	.71	Kreemer et al., 2014
loveless_meade	X	X	147	19.1	.64	Loveless and Meade, 2011
mccaffrey	X	X	93	17.6	.60	McCaffrey et al., 2013
parsons	O	X	92	24.4	.42	Parsons et al., 2006
shen	X	X	91	12.7	.74	Shen et al., 2015
smith_konter	X	X	171	14.0	.63	Smith-Konter and Sandwell, 2009
tape	O	X	73	26.1	.66	Tape et al., 2009
tong	X	X	173	15.4	.60	Tong et al., 2013
zeng	X	X	139	14.0	.72	Zeng and Shen, 2016a

The rms column is second invariant of the strain shown in Figure 2. The SHmax is the standard deviation in degrees of the difference between the orientation of the direction of maximum compression and SHmax from seismic moment tensors [Yang and Haukkson, 2013]. The corr column is the average of the cross correlation of each model with all the other models in the set. Boxes shaded in grey were not used in the consensus CGM model because of the following reasons. The bormann_hammond model did not completely cover the region of interest. The becker, parsons, and tape models have no velocity grid. The hackl, parsons, and tape models had very poor fit to SHmax.

1. Evaluation
    1.1. Second invariant and model roughness
    1.2. Fits to cross-fault strain-rate measurements
    1.3. Second invariant correlation matrix
    1.4. Shmax
2. Winnowing
    2.1. Select candidate models
    2.2. Perform correlation on model subset
3. Polishing
    3.1. Polish each of the candidate models with the zeng_shen data
    3.2. Perform cross-correlation analysis
    3.3. Perform sum and difference analysis on velocities
    3.4. Perform sum and difference analysis on strain

3.5. Compare with seismicity and Shmax

4. The Model

4.1. East and North Velocity grids and rms grids

4.2. Strain tensor grids and uncertainties

4.3. GMT scripts for computing and plotting other products

Table 2. Analysis of 10 models used for the CGM

	GPS mm/yr		MEAN model mm/yr		second invariant nanostrain/yr
model	rms	rms masked	rms	rms masked	
mean	0.92	0.85	-	-	119
zeng	1.04	0.94	0.33	0.13	139
gpsgridder	1.03	0.95	0.37	0.16	109
bird	1.02	0.95	0.33	0.16	184
smith_konter	1.04	0.92	0.35	0.17	171
holt	0.99	0.89	0.26	0.16	124
tong	1.07	0.98	0.28	0.18	173
loveless_meade	1.08	0.96	0.28	0.21	145
mccaffrey	0.85	0.74	0.31	0.27	93
shen	0.81	0.74	0.64	0.27	91
kreemer	1.11	0.96	0.44	0.36	147

Note that each of the models was adjusted to match the 1339 velocity vectors in the region (see Figure 1). This was done using a remove/interpolate/restore method [Sandwell and Wessel, 2016]. The interpolation method does not fit the GPS vectors exactly with the typical rms difference is 1 mm/yr. and slightly smaller when the points in the creeping section are excluded. The rms difference between the mean model and the individual models was also computed with and without the masked areas shown in Figure 7. The rougher models fit the mean model better than the smoother models.

Appendix A Strain Rate Above a Buried Dislocation

We use a very simple model to describe the expected strain rate near a straight strike-slip fault that is locked from the surface to a depth D and freely slipping at a velocity V at greater depth.

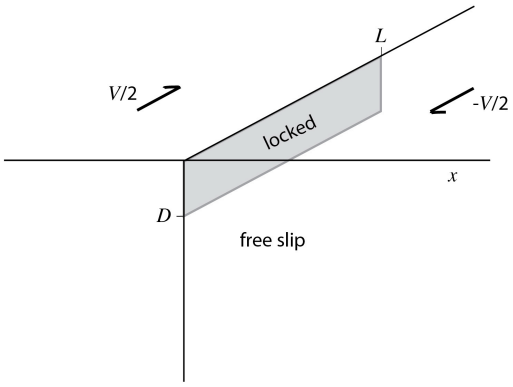

Figure A1. Schematic diagram of idealized strike-slip fault during the interseismic part of the earthquake cycle.

The velocity as a function of distance x across the fault is given by the standard arctangent solution [*Turcotte and Schubert*, 2014]

$$v(x) = \frac{V}{\pi} \tan^{-1} \frac{x}{D}. \tag{A1}$$

The strain rate ε is the derivative of the velocity with respect to x and is

$$\varepsilon(x) = \frac{V}{\pi D} \frac{1}{1 + \left(\frac{x}{D}\right)^2}. \tag{A2}$$

Finally the seismic moment accumulation rate $\dot{M}$ per unit length of fault L is

$$\frac{\dot{M}}{L} = \mu D V \tag{A3}$$

where μ is the shear modulus. For example to estimate the strain rate across the Carrizo and Imperial faults we fit a two-parameter model to the GPS velocity data and then use the parameters $[D,V]$ in equation A2 to estimate strain rate as shown in Figures 1 and 4.

Appendix B Construction of Matching Grids of Velocity and Strain Rate Tensor

We used a very standard approach to convert the 15 contributions of velocity and/or strain rate tensor into models that could be compared directly. The analysis was entirely 2-dimensional so we have not considered the vertical velocity or vertical components of the strain rate tensor. Typically the model was provided on a uniform grid. For example the kreemer contribution was a file consisting of columns of longitude x, latitude y, east velocity v_x, and north velocity v_y provided in mm/yr on a 0.02˚ grid. In all cases we regridded the velocity and strain rate fields on a 0.01˚ interval which corresponds roughly to a 1 km spacing. A typical GMT command sequence is:

```
awk '{print $1-360, $2, $3}' < vel_0.02_WUS_NA.gmt > llve.dat
awk '{print $1-360, $2, $4}' < vel_0.02_WUS_NA.gmt > llvn.dat
surface llve.dat -T.5 -R-125./-114./30.5/42.0 -I.01 -V -r -Gve_tot.grd
surface llvn.dat -T.5 -R-125./-114./30.5/42.0 -I.01 -V -r -Gvn_tot.grd
```

While this is interval probably finer than needed to represent the data, oversampling is needed for accurate computation of derivatives. We compute the strain rate using the standard formulas:

$$\varepsilon_{xx} = \frac{\partial v_x}{\partial x}, \quad \varepsilon_{yy} = \frac{\partial v_y}{\partial y}, \quad \varepsilon_{xx} = \frac{1}{2}\left(\frac{\partial v_x}{\partial y} + \frac{\partial v_y}{\partial x}\right).$$

A GMT command sequence is:

```
grdgradient ve_tot.grd -Gvxx.grd -A270 -fg -V
grdgradient ve_tot.grd -Gvxy.grd -A180 -fg -V
grdgradient vn_tot.grd -Gvyx.grd -A270 -fg -V
grdgradient vn_tot.grd -Gvyy.grd -A180 -fg -V
```

```
#
grdmath vxx.grd 1000. DIV = exx.grd
grdmath vyy.grd 1000. DIV = eyy.grd
grdmath vxy.grd vyx.grd ADD 2000. DIV = exy.grd
```

Note GMT uses a local flat-earth approximation to convert degrees to meters. For the analysis we compute three derivative products from the strain rate tensor. The first is the second invariant of strain rate given by

$$\varepsilon_{II} = \left(\varepsilon_{xx}^2 + \varepsilon_{yy}^2 + 2\varepsilon_{xy}^2\right)^{1/2}.$$

A GMT command sequence to compute second invariant strain rate in nanoradians per year is:

```
grdmath exx.grd SQR = exx2.grd
grdmath eyy.grd SQR = eyy2.grd
grdmath exy.grd SQR 2 MUL = exy2.grd
grdmath exx2.grd exx2.grd ADD exx2.grd ADD SQRT 1.e9 MUL = secinv.grd
```

The second are the two components of the principal strain rate given by

$$\varepsilon_{1,2} = \frac{\varepsilon_{xx} + \varepsilon_{yy}}{2} \pm \frac{1}{2}\left\{\left(\varepsilon_{xx} - \varepsilon_{yy}\right)^2 + 4\varepsilon_{xy}^2\right\}^{1/2}.$$

The first term in (A2) is the dilitation rate (extension is positive) and the shear strain rate. The third is the angle of the extensional deformation axis (counterclockwise with respect to x) that we will compare with SHmax. This is given by

$$\alpha = \frac{1}{2}\tan^{-1}\left(\frac{2\varepsilon_{xy}}{\varepsilon_{xx} - \varepsilon_{yy}}\right).$$

A GMT command is:

```
grdmath 2 exy.grd MUL exx.grd eyy.grd SUB ATAN2 2 DIV = a.grd
```

References

Bennett, R., W. Rodi, and R. Reilinger, Global Positioning System constraints on fault slip rates in southern California and northern Baja, Mexico, J. Geophys. Res., 101, B10, 21943-21960, 1996.

Bird, P., Long-term fault slip rates, distributed deformation rates, and forecast of seismicity in the western United States from joint fitting of community geologic, geodetic, and stress-direction datasets, J. Geophys. Res., 114, B11403, doi:10.1029/2009JB006317, 2009.

Crowell, B. W., Y. Bock, D. T. Sandwell, and Y. Fialko (2013), Geodetic investigation into the deformation of the Salton Trough, J. Geophys. Res. Solid Earth, 118, doi:10.1002/jgrb.50347.

Dixon, T., J. Decaix, F. Farina, K. Furlong, R. Malservisi, R. Bennett, F. Suarez,-Vidal, J. Flecher, and J. Lee, Seismic cycle and rheological effects on estimation of present-day slip rates for the Agua Blanca and San Miguel-Vallecitos faults, northern Baja California, Mexico, J. Geophys. Res., 107, B10, 2226, doi:10.1029/2000JB000099, 2002.

Field, E. H., Arrowsmith, R. J., Biasi, G. P., Bird, P., Dawson, T. E., Felzer, K. R., ... & Zeng, Y. (2014). Uniform California Earthquake Rupture Forecast, Version 3 (UCERF3)−The Time‐Independent Model. Bulletin of the Seismological Society of America, 104(3), 1122-1180.

Flesch, L. M., Holt, W. E., Haines, A. J., & Shen-Tu, B. (2000). Dynamics of the Pacific-North American plate boundary in the western United States. Science, 287(5454), 834-836.

Freed, A. M., S. T. Ali, and R. Burgmann, Evolution of stress in Southern California for the past 200 years from coseismic, postseismic and interseismic stress changes, Geophys. J. Int.,169, p. 1164-1179, 2007.

Genrich, J. F., Y. Bock, and R. G. Mason, Crustal deformation across the Imperial Fault: Results from kinematic GPS surveys and trilateration of a densely-spaced, small-aperture network, J. Geophys. Res., 102, 4985– 5004, 1997.

González-Ortega, J. A., Y. Fialko, D. Sandwell, F. A. Nava Pichardo, J. Fletcher Mackrain, J. J. Gonzalez Garcia, B. Lipovski , M. Floyd y G. Funning. El Mayor-Cucapah (Mw 7.2) earthquake: Early near-field postseismic deformation from InSAR and GPS observations. Journal of Geophysical Research. Solid Earth. 119(2): 1482-1497. 2014.

Hackl, M., R. Malservaisi, and S. Wdowinski, Strain pattern from dense GPS networks, Nat. Hazards Earth Syst., 9., 1177-1187, 2009.

Hauksson, E., and D. Sandwell (2013), Comparison of SHmax orientations from stress inversions of focal mechanisms with 17 different strain models determined from GPS data in southern California: Contribution to the SCEC stress model, SCEC Annual Meeting, poster 087.

Hearn, E., K. Johnson, D. Sandwell, and W. Thatcher, SCEC UCERF workshop report: http://www.scec.org/workshops/2010/gps-ucerf3/FinalReport_GPS-UCERF3Workshop.pdf, 2010.

Johnson, K., P. Bird, Y. Zeng, W. Thatcher, T. Dawson, R. Weldon, R. McCaffrey, W.C. Hammond, J. Bormann, T. Herring, 2013, Geodetically-derived deformation models for UCERF3, report for the Working Group On California Earthquake Probabilities, available at http://wgcep.org.

Kreemer, C., G. Blewitt, W. C. Hammond, and H. P. Plang, A high-resolution strain rate tensor model for the western U. S., EarthScope National Meeting 2009, Boise, ID, 2009.

Kreemer, C., G. Blewitt, and E. C. Klein (2014), A geodetic plate motion and Global Strain Rate Model, Geochem. Geophys. Geosyst., 15, 3849–3889, doi:10.1002/2014GC005407.

Lindsey, E. O., Fialko, Y., Bock, Y., Sandwell, D. T., & Bilham, R. (2014). Localized and distributed creep along the southern San Andreas Fault. Journal of Geophysical Research: Solid Earth, 119(10), 7909-7922.

Loveless, J. P., & Meade, B. J. (2011). Stress modulation on the San Andreas fault by interseismic fault system interactions. Geology, 39(11), 1035-1038.

Lyons, S. N., Y. Bock, and D. T. Sandwell, Creep along the Imperial Fault, southern California, from GPS measurements, J. Geophys. Res., 107(B10), 2249, doi:10.1029/2001JB000763, 2002.

McCaffrey, R., Block kinematics of the Pacific–North America plate boundary in the southwestern United States from inversion of GPS, seismological, and geologic data, J. Geophys. Res., 110, B07401, doi:10.1029/2004JB003307, 2005.

McCaffrey, R., King, R. W., Payne, S. J., & Lancaster, M. (2013). Active tectonics of northwestern US inferred from GPS‐derived surface velocities. Journal of Geophysical Research: Solid Earth, 118(2), 709-723.

McCaffrey, R, P. Bird, J. Bormann, K.M. Haller, W.C. Hammond, W.R. Thatcher, R.E. Wells, and Y. Zeng (2013). NSHMP block model of Western United States active tectonics, Appendix A, U.S. Geological Survey Open-File Report 2013–1293, p. 27–38.

Meade, B.J., and B.H. Hager, Block models of crustal motion in southern California constrained by GPS measurements, J. Geophys. Res., 110, doi:10.1029/2004JB003209, 2005a.

Meade, B.J., and B.H. Hager, Spatial localization of moment deficits in southern California, J. Geophys. Res., 110, doi:10.1029/2004JB003331, 2005b.

Parsons, T., Tectonic stressing in California modeled from GPS observations, J. Geophys. Res. 111, doi:10.1029/2005JB003946, 2006.

Parsons, T., K.M. Johnson, P. Bird, J.M. Bormann, T.E. Dawson, E.H. Field, W.C. Hammond, T.A. Herring, R. McCaffrey, Z.-K. Shen, W.R. Thatcher, R.J. Weldon and Y. Zheng, 2013, Appendix C- Deformation models for UCERF3, USGS Open-File Report, v. 2013-1165, 66 pp., http://pubs.usgs.gov/of/2013/1165/pdf/ofr2013-1165_appendixC.pdf.

Petersen, M. D., Mueller, C. S., Frankel, A. D., & Zeng, Y. Appendix J: Spatial Seismicity Rates and Maximum Magnitudes for Background Earthquakes, USGS Open File Report 2007-1437J, 2008.

Petersen, M. D., Y. Zeng, K. M. Haller, R. McCaffrey, W. C. Hammond, P. Bird, M. Moschetti, Z. Shen, J. Bormann, and W. Thatcher [2014] Geodesy- and

geology-based slip-rate models for the Western United States (excluding California) national seismic hazard maps, U.S. Geol. Surv. Open-File Rep., 2013-1293, 38 pages doi.org/10.3133/ofr20131293.

Platt J. P. and T. W. Becker, Where is the real transform boundary in California?, Geochem. Geophys. Geosyst., 11, Q06012, doi:10.1029/2010GC003060, 2010.

Platt, J. P., B. Kaus, and T. Becker, The mechanics of continental transforms: An alternative approach with applications to the San Andreas system and the tectonics of California, Earth Planet. Sci. Lett., v. 274, p. 380-391, 2008.

Shen, Z.-K., D. Jackson, and B. Ge, Crustal deformation across and beyond the Los Angeles Basin from geodetic measurements, J. Geophys. Res., 101, 27957–27980, 1996.

Shen, Z. K., Jackson, D. D., & Kagan, Y. Y. (2007). Implications of geodetic strain rate for future earthquakes, with a five-year forecast of M5 earthquakes in southern California. Seismological Research Letters, 78(1), 116-120.

Shen, Z.-K., R.W. King, D.C. Agnew, M. Wang, T.A. Herring, D. Dong, and P. Fang (2011). A unified analysis of crustal motion in southern California, 1970-2004: The SCEC crustal motion map: *Journal of Geophysical Research*, v. 116, B11402, doi: 10.2019/2011JB008549.

Shen, Z. K., Wang, M., Zeng, Y., & Wang, F. (2015). Optimal interpolation of spatially discretized geodetic data. Bulletin of the Seismological Society of America, **105**, 2117-2127.

Simpson, R. W., W. Thatcher, J. C. Savage, Using cluster analysis to organize and explore regional GPS velocities, Geophys. Res. Lett., 39, DOI: 10.1029/2012GL052755, 2012.

Smith-Konter, B., D. T. Sandwell, Stress evolution of the San Andreas Fault System: recurrence interval versus locking depth, Geophys. Res., Lett., 35, L13304, doi:10.1029/2009GL037235, 2009.

Tape, C., P. Muse, M. Simons, D. Dong, and F. Webb, Multiscale estimation of GPS velocity fields, Geophys. J. Int., 179, 945-971, 2009.

Tong, X., D. T. Sandwell, and B. Smith-Konter (2013), High-resolution interseismic velocity data along the San Andreas Fault from GPS and InSAR, J. Geophys. Res.; Solid Earth, 118, doi:10.1029/2012JB009442.

Tymofyeyeva, E., & Fialko, Y. (2015). Mitigation of atmospheric phase delays in InSAR data, with application to the eastern California shear zone. Journal of Geophysical Research: Solid Earth, 120(8), 5952-5963.

Wei, M., D. T. Sandwell, and B. Smith-Konter, Optimal combination of InSAR and GPS for measuring interseismic crustal deformation, J. Adv. in Space Res. doi:10.1016/j.asr.2010.03.013, 2010.

Yang, W., and E. Hauksson (2013), The tectonic crustal stress field and style of faulting along the Pacific North America Plate boundary in Southern California, Geophys. J. Int., 194, doi:10.1093/gji/ggt113.

Zeng Y. and Z.-K. Shen (2016a). A Fault-Based Model for Crustal Deformation, Fault Slip Rates and Off-Fault Strain Rate in California, BSSA, 106(2), doi:10.1785/0120140250.

Zeng Y. and Z.-K. Shen (2016b). A Fault-Based Model for Crustal Deformation in the Western United States Based on a Combined Inversion of GPS and Geologic Inputs, BSSA, in press.